Chinese Chemical Letters 36 (2025) 110817

Contents lists available at ScienceDirect

Chinese Chemical Letters

journal homepage: www.elsevier.com/locate/cclet

# Asymmetrical carbazole-benzonitrile-based TADF emitters designed by alternate donor-acceptor strategy

Zhaoyue Lü[b,1], Tiantian Chai[a,1], Yichao Jin[b], Xiao Wang[b], Ye Zou[c,*], Lijiang Zhang[b], Jiankang Feng[a], Mengtong Zhang[a], Shuo Wang[a], Chichong Lu[d,*], Guofan Jin[a,*]

[a] School of Pharmacy, Jiangsu University, Zhenjiang 212013, China
[b] School of Physics, East China University of Science and Technology, Shanghai 200237, China
[c] Laboratory of Organic Solids, Institute of Chemistry, Chinese Academy of Sciences, Beijing 100190, China
[d] Department of Chemistry, College of Light Industry Science and Engineering, Beijing Technology and Business University, Beijing 100048, China

ARTICLE INFO

*Article history:*
Received 18 September 2024
Revised 27 December 2024
Accepted 2 January 2025
Available online 2 January 2025

*Keywords:*
Delayed fluorescence
Linear D-A-D structure
Localized excited state
Delocalized charge transfer state
Spin-orbital coupling

ABSTRACT

A pair of asymmetric rigid carbazole-benzonitrile-based emitters were synthesized by strategically alternating donor and acceptor groups along the molecular edges. The spin-flip process is accelerated by both the formation of localized and delocalized charge transfer states due to linearly positioned donors and strong spin-orbital coupling between different excitation feature of the lowest singlet and triplet excited states. This molecular architecture results in a remarkable short delayed lifespan of around 100 ns. The application of the two emitters in organic light-emitting diodes (OLEDs) achieves the highest external quantum efficiencies of 13.0% for the green emitter and 9.1% for the sky-blue emitter. Impressively, these devices maintain their high efficiency even at high luminance levels. The sustained efficiency is ascribed to the effective suppression of exciton quenching by substantially shortening delayed lifespan. These findings underscore the practical utility of the molecular design strategy that incorporates alternate donor and acceptor groups at the molecular periphery for shortening delayed fluorescence lifetime, and hold great promise for the development of high-performance OLEDs.



Thanks to the distinct features of self-luminescence, flexibility, and high contrast, organic light-emitting diodes (OLEDs) have been widely applied in the fields of consumer electronic displays [1,2], augmented/virtual reality [3,4], biomedicine [5,6], and so on. As the third-generation emissive materials, thermally activated delayed fluorescence (TADF) emitters are at the forefront of OLED research because they are free of noble metals and can harvest 100% exciton for emission due to up-conversion from the lowest triplet ($T_1$) to singlet ($S_1$) excited states *via* reverse intersystem crossing (RISC) mechanism [7,8]. The key to this process is a small energy gap between the $S_1$ and $T_1$ states ($\Delta E_{ST}$). Achieving a small $\Delta E_{ST}$ without sacrificing photoluminescence (PL) efficiency is a challenge. The classical approach to this challenge involves constructing donor-acceptor (D-A) type molecules [9,10]. Since Adachi's pioneering work [11], there has been an explosion of innovation, leading to the development of numerous highly efficient TADF emitters and significant advancements in the field [12–17].

Carbazole-benzonitrile derivatives (CzBNs) stand out as a class of exemplary TADF emitters. Some of the CzBNs emitters feature a single type of donor, termed as homo-donor structures [18–20], and some are hetero-donor structures, which incorporate two or more distinct donor groups [21–25]. The latter has garnered increasing interest due to their potential to reduce the delayed lifetime and improve device stability. Despite the impressive efficiency and stability of CzBNs, TADF OLEDs based on these materials often encounter a significant efficiency roll-off, which is primarily attributed to exciton quenching [26–29]. To overcome this challenge and unlock the full potential of CzBNs in high-performance OLEDs, a rational molecular design is essentially required.

Up until now, the majority of CzBN-based TADF molecules have featured symmetric rigid structures [18–20], while asymmetric rigid structures have been less explored [22]. In this contribution, we introduce a novel approach by designing a pair of hetero-donor-based asymmetric rigid CzBN molecules. These molecules are characterized by alternating donor and acceptor moieties at their periphery. Specifically, carbazole (Cz) and modified-Cz

* Corresponding authors.
*E-mail addresses:* zouye@iccas.ac.cn (Y. Zou), luchichong@btbu.edu.cn (C. Lu), organicboron@ujs.edu.cn (G. Jin).
[1] These authors contributed equally to this work.

https://doi.org/10.1016/j.cclet.2025.110817
1001-8417/

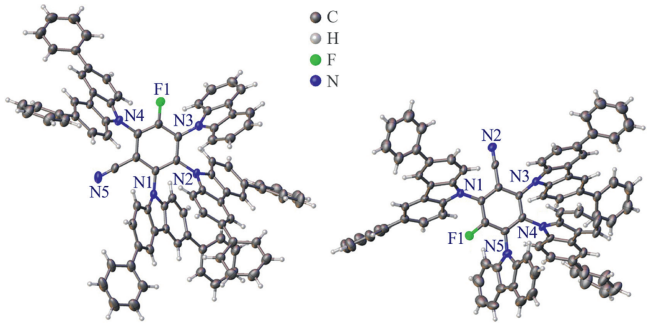


**Fig. 1.** X-ray single crystal diffraction structures of the two compounds: (left) 3DPh and (right) 2DPh.

moieties groups serve as donors, while cyano (CN) and fluorine (F) units act as acceptors. This configuration offers several advantages: (1) The inclusion of a second or third donor enhances the interplay between charge transfer (CT) and localized excited (LE) states, thereby promoting RISC [21,24,30]. (2) The linear arrangement of the D-A-D system facilitates the formation of delocalized excited states and alleviates structural relaxation, and further boosts RISC and luminous efficiency [30]. (3) The asymmetric rigid structures deliver significant steric hindrance, which minimizes molecular vibration and suppresses non-radiative deactivation of excitons. Based on such a motif, (2*S*,3*R*,4*R*,6*R*)–4-(9*H*-carbazol-9-yl)–2,3,6-tri(3,6-diphenyl-9*H*-carbazol-9-yl)–5-fluoro-bezonitrile (referred as 3DPh) and (2*R*,4*R*,5*R*,6*S*)–4-(9*H*-carbazol-9-yl)–2,6-bis(3,6-diphenyl-9*H*-carbazol-9-yl)–3-fluoro-5-(3-phenyl-9*H*-carbazol-9-yl) benzonitrile (referred as 2DPh) were synthesized here. Detailed synthesis procedures and nuclear magnetic resonance (NMR) characterizations are presented in Scheme S1 and Figs. S1-S4 (Supporting information).

To get insight into molecular structural properties, the interior structures of the compounds were visualized by using X-ray single crystal diffraction (SC-XRD). The SC-XRD results reveal that the new compounds consist of a central benzene ring, with Cz and phenyl-modified Cz groups positioned at the periphery of this central benzene ring (Fig. 1). The three-dimensional spatial conformation and primary crystallographic data of these compounds are further detailed in Fig. S5 and Table S1 (Supporting information). The observations indicate that the two individual crystals are part of asymmetric polyaromatic ring structures, providing valuable insight into the molecular architecture and potential implications for their physical and chemical properties.

Both the compounds show similar absorption spectra, as shown in Figs. 2a and b. The absorption peaked at around 290 nm is attributed to the $\pi-\pi^*$ transition of Cz or modified-Cz donors. Additionally, the relatively weak and broad absorption bands in the range of 330–450 nm are indicative of intramolecular charge transfer (ICT) transitions from DPhCz/PhCz donors to BN acceptors. To further elucidate the origins of these broad absorption bands, we employed Gaussian fitting to dissect the spectra between 280 nm and 500 nm into three distinct components. The decomposed curves peak approximately at 290, 350 and 380 nm, respectively, corresponding to the $\pi-\pi^*$ band of the Cz groups, the normal, and novel CT bands. Similar to the cases of 4CzBN and 5CzBN [30], the normal and novel CT bands are believed to arise from the formation of localized CT ($^{lo}$CT) and delocalized CT ($^{de}$CT) states. This is because the two compounds are capable of forming a linear D-A-D structure [30], specifically with the BN unit and DPhCz groups at the 3- and 6-positions for 3DPh, BN and 2-DPhCz and 5-PhCz groups for 2DPh. The HOMO energy levels of the two compounds are determined from measuring their pristine films using ultraviolet photoelectron spectroscopy (UPS) [31,32]. As shown

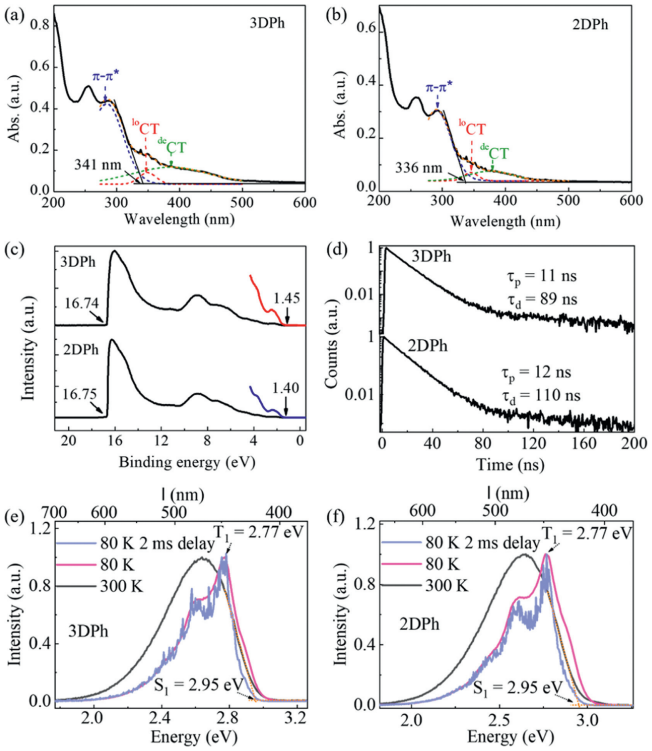


**Fig. 2.** Absorption spectra with Gaussian fitting curves of (a) 3DPh and (b) 2DPh. (c) UPS spectra and (d) transient PL decays of 3DPh and 2DPh. PL spectra at 300 K, 80 K, and 80 K with 2 ms delay of (e) 3DPh and (f) 2DPh.

in Fig. 2c, the HOMO levels are found to be −5.92 eV for 3DPh and −5.87 eV for 2DPh. By combining these HOMO levels with the optical bandgaps ($E_g$) determined from the absorption spectra, the corresponding LUMO levels are estimated to be −2.28 eV for 3DPh and −2.18 eV for 2DPh.

The transient PL decay profiles for the emission of both compounds in 2,2-dimethyltetrahydrofuran (2Me-THF) were monitored at 300 K. As presented in Fig. 2d, both compounds exhibit bi-exponential decay, characterized by a nano-second-scale prompt component (~10 ns) and a notably short sub-microsecond-scale delayed component (~100 ns) by fitting with a biexponential decay function, indicating highly efficient $T_1$-to-$S_1$ spin-flip transition. The steady state PL spectra of each compound were also measured in 2Me-THF solution (Figs. 2e and f). Both compounds exhibit almost identical PL spectra, with broad and structureless emissions peaking at 470 nm at 300 K, which declares CT feature of $S_1$ states ($^1$CT$_1$). In contrast, the PL spectra at 80 K reveal two distinct peaks at 448 and 475 nm, delivering a well-resolved vibronic structure. These two peaks are likely attributed to different excited triplet states. The peak at 448 nm might stem from $^3$LE state of modified-Cz moieties [21], while the peak at 475 nm should originate from the CT state. The phosphorescence emission is confirmed by the virtually identical prompt and delayed PL spectra at 80 K, manifesting that the $T_1$ state is a mixed state of LE and CT characters, as expected in hetero-donor systems [21,24,30]. According to El-Sayed rule [33,34], spin-orbital coupling (SOC) between $S_1$ and $T_1$ is permitted as their distinct excited state features and the change in spatial orbital angular momentum [35], which accelerates delayed fluorescence and bring about a remarkably short delayed lifetime. From the spectra, the energies of $S_1$ and $T_1$ states for the two emitters were calculated to be 2.95 and 2.77 eV, respectively, yielding a small $\Delta E_{ST}$ of 0.18 eV.

Theoretical computations based on density function theory (DFT) were carried out to examine the geometrical and elec-

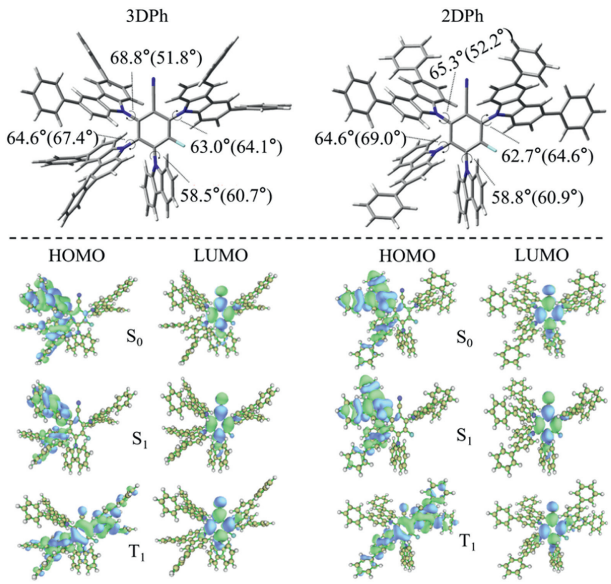


**Fig. 3.** The structures of the 3DPh and 2DPh compounds (upper, the values in parentheses are crystal data), and their calculated FMO and NTO distributions *via* Gaussian at B3LYP/6–31G(d) level (lower).

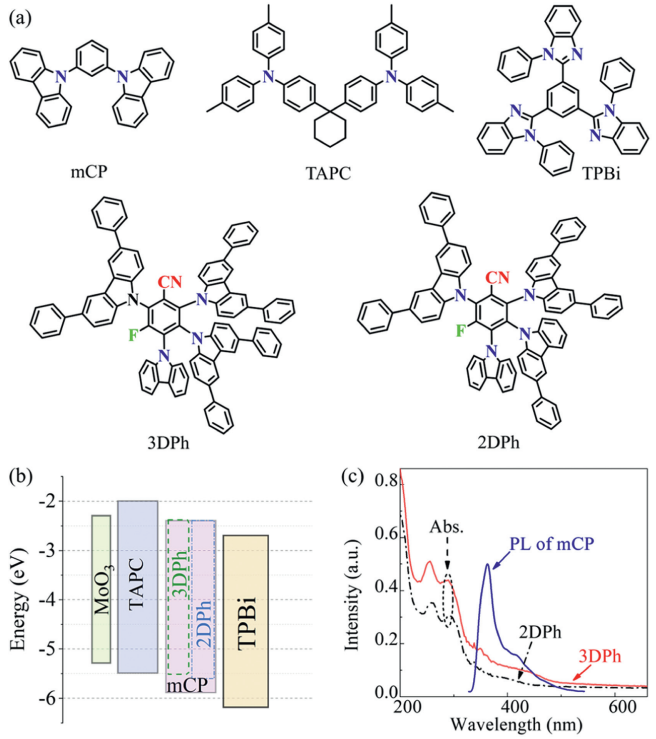


**Fig. 4.** (a) The molecular structures and (b) energy level alignment of organic semiconductors in this study. (c) PL spectrum of mCP and absorption of the 3DPh and 2DPh emitters.

tronic characteristics of the two compounds. Fig. 3 shows the optimized ground state ($S_0$) structures using Gaussian software at the B3LYP/6–31G(d) level [36]. In both emitters, the dihedral angles between the Cz units and the central phenyl ring are notably large ($>50^{\circ}$), consistent with the observations from the crystal structures. Additionally, Fig. 3 also illustrates the frontier molecular orbital (FMO) distributions of their $S_0$ states of the compounds. The computed lowest unoccupied molecular orbitals (LUMOs) of both compounds are principally located on the BN unit, while the highest occupied molecular orbitals (HOMOs) are predominantly situated at the 2-, 3-sites or 5-, 6-sites modified-Cz moieties, which are spatially well separated from their LUMOs and weakly overlapped with LUMOs at the central benzene ring. Due to this effective spatial separation between the FMOs, the exchange integral is expected to be small, and the excitation of HOMO-to-LUMO is assumed to be an ICT excitation. It is also noteworthy that the HOMO distribution in 3DPh is more delocalized and extends considerably to the peripheral phenyl of the DPhCz group at the 3-position compared to 2DPh. This increased delocalization could imply that 3DPh may exhibit higher radiative efficiency.

Excited state ($S_1$ and $T_1$) structures and natural transition orbitals (NTOs) [37] for the two compounds were further calculated by using time-dependent DFT (TD-DFT) at a B3LYP/6–31G(d) level. Similar to $S_0$ state, the highest occupied NTOs of the $S_1$ states are distributed on 2-, 3-positions (or 5-, 6-positions) of the modified Cz units for both molecules, while the lowest unoccupied NTOs are delocalized over the BN unit (Fig. 3). Interestingly, for the $T_1$ states, the highest occupied NTOs are delocalized across a linearly positioned pair of modified-Cz units (*i.e.*, 3-, 6-positions or 2-, 5-positions) along with the BN core. The $S_1$ and $T_1$ states exhibit characteristics of CT and hybrid local charge transfer (HLCT), respectively, which is in good agreement with experimental observations. A linear D-A-D structure facilitates the formation of delocalized excited state and promotes RISC [30]. The calculated energy gaps of $\Delta E_{ST}$ are 0.094 eV for 3DPh and 0.110 eV for 2DPh, indicating the potential for efficient TADF performance. Both emitters have similar HOMO and LUMO values, although there is a deviation between the experimental results and the computed values. A summary of the calculated and experimental parameters for the two emitters is presented in Table 1, showing a good overall consistency between the two sets of data.

The electroluminescent (EL) performance of devices incorporating 3DPh and 2DPh as the emissive materials were studied. For the host material, 1,3-bis(carbazol-9-yl)benzene (mCP) was chosen due to its high triplet energy ($T_1 = 2.90$ eV), which is compatible with the emitters. The molecular structures and energy level alignment of the organic materials used in this study are illustrated in Figs. 4a and b, respectively. The PL spectrum of mCP overlaps well with the absorption spectra of the two emitters (Fig. 4c), indicating efficient energy transfer from the mCP host to the emitters. Di-[4-(*N*,*N*-ditolyl-amino)-phenyl]cyclohexane (TAPC) and 1,3,5-tris(1-phenyl-1*H*-benzimidazol-2-yl)benzene (TPBi) were respectively selected as the hole and electron transporting layers due to their outstanding carrier mobility. The detailed device structure is ITO/$MoO_3$ (3 nm)/TAPC (50 nm)/mCP:emitter (*x* wt%, 20 nm)/TPBi (60 nm)/LiF (0.8 nm)/Al (150 nm). Here, $MoO_3$ and LiF serve as the hole and electron injection layers, respectively, and the doping concentration of each emitter was optimized. With a 5% increment, the doping concentration of the emitters in mCP (*x*%) was incrementally increased from 5% to 20%. The devices with emitters of 3DPh and 2DPh were labelled as sets A and B, respectively. The resultant device performance can be found in Figs. S6 and S7 (Supporting information), with the main parameters summarized in Tables S2 and S3 (Supporting information).

As shown in Fig. S6, the devices based on 3DPh exhibit nearly concentration-independent current density-voltage (*J*–*V*) characteristics and maintain a consistent turn-on voltage of $4.60 \pm 0.06$ V (at 10 cd/m$^2$). The luminance-voltage (*L*–*V*) profiles indicate a shift towards lower voltages with increasing doping content. The optimum 3DPh-based device with a doping content of 15% achieves a maximum luminance of 47,042 cd/m$^2$ and peak efficiencies of 37.5 cd/A, 13.0% and 21.9 lm/W. Fig. S7 illustrates that for the 2DPh-based devices, the current density increases with higher doping

**Table 1**
The experimental (Ex) and calculated (Cal) parameters of the two emitters.

| Compd. | | $S_1$ (eV) | $T_1$ (eV) | $\Delta E_{ST}$ (eV) | HOMO (eV) | LUMO (eV) | $E_g$ (eV) | $\lambda_{em}$ (nm) |
|---|---|---|---|---|---|---|---|---|
| 3DPh | Ex | 2.64 | 2.77 | 0.18 | −5.92 | −2.28 | 3.64 | 470 |
| | Cal | 2.567 | 2.473 | 0.094 | −5.439 | −2.313 | 3.122 | 483 |
| 2DPh | Ex | 2.64 | 2.77 | 0.18 | −5.87 | −2.18 | 3.69 | 470 |
| | Cal | 2.617 | 2.507 | 0.117 | −5.439 | −2.313 | 3.126 | 474 |

**Table 2**
The key properties of the OLED devices with different emitters.

| Emitter | $V$ at 10 cd/m$^2$ (V) | $L_{max}$ (cd/m$^2$) | Maxmium $\eta_{CE}/\eta_{EQE}/\eta_{PE}$ ((cd/A)/%/(lm/W)) | $\eta_{CE}/\eta_{EQE}/\eta_{PE}$ at 1000 cd/m$^2$ ((cd/A)/%/(lm/W)) | $\lambda_{peak}$ (nm) [a] |
|---|---|---|---|---|---|
| 3DPh (15 wt%) | 4.63 | 47,042 | 37.5/13.0/21.9 | 36.2/12.6/15.6 | 506 |
| 2DPh (20 wt%) | 5.13 | 24,404 | 18.0/9.1/10.2 | 15.0/8.0/5.6 | 487 |

[a] Measured at 1000 cd/m$^2$.

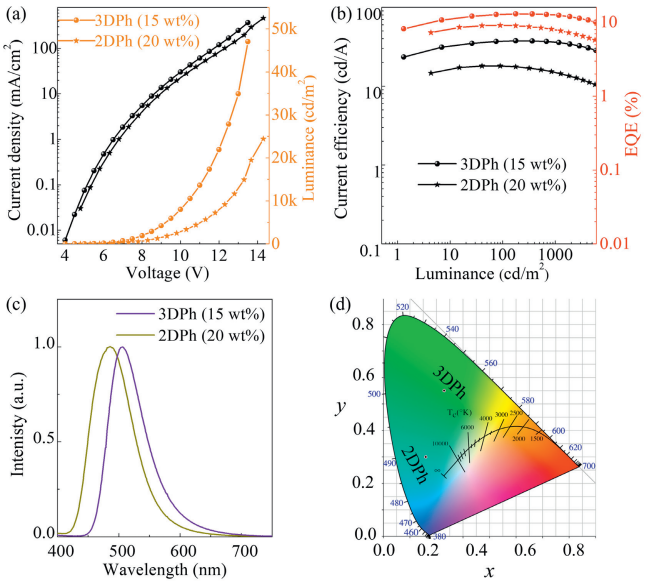


**Fig. 5.** EL characteristics of the optimized devices with the two emitters: (a) *J*–*V*–*L*, (b) $\eta_{CE}$–*L*–$\eta_{EQE}$. (c) EL spectra and (d) CIE coordinates at 1000 cd/m$^2$.

contents under a fixed voltage. Similarly, the *L*–*V* profiles show a reduction in driving voltage as the doping content rises, from 5.88 V for 5%-doped device to 5.13 V for the 20%-doped device at a constant luminance of 10 cd/m$^2$. The device doped with 20% 2DPh delivers the best performance, with the lowest driving voltage (5.13 V at 10 cd/m$^2$), the maximum luminance (24,404 cd/m$^2$ at 14.7 V) and the highest efficiencies (18.0 cd/A, 9.1%, and 10.2 lm/W). One also notes that the EL spectra shown in Figs. S6d and S7d slightly redshift when the doping level rises from 5 wt% to 20 wt%, which may be attributed to the emission of aggregation states caused by stronger intermolecular interaction [38].

Fig. 5 and Table 2 present the EL characteristics and key parameters of the devices with the optimal content of emitters, *i.e.*, ITO/$MoO_3$/TAPC/mCP: 15 wt% 3DPh/TPBi/LiF/Al and ITO/$MoO_3$/TAPC/mCP: 20 wt% 2DPh/TPBi/LiF/Al. Because of the substituent effect of DPhCz group at the 3-position, the 3DPh-based device outperforms the 2DPh-based device in terms of current density, luminance, and efficiency (Figs. 5a and b). Both devices demonstrate a remarkable low efficiency roll-off. For the 3DPh-based device, the EQE maintains 96% and 79% of its maximum value at 1000 and 5000 cd/m$^2$, respectively (Fig. 5b). For the 2DPh-based device, the corresponding values are 87% and 65%. This suppressed roll-off is likely due to the short-delayed lifespan (100 ns), which moderates the density of $T_1$ states in emissive layer and alleviates the annihilation of $T_1$ states [8,21,39]. The reduction in donor strength of the PhCz group relative to the DPhCz gives rise to a considerable blueshift of 2DPh-based device compared to the 3DPh-based device (Fig. 5c). The 2DPh-based device exhibits a sky-blue emission with a peak wavelength of 487 nm and Commission Internationale de lÉclairage (CIE) coordinates of (0.16, 0.31), while the 3DPh-based device has a peak emission at 506 nm with CIE coordinates of (0.23, 0.55) (Fig. 5d).

In conclusion, we have successfully synthesized a couple of CzBN-based emitters featuring asymmetrical rigid structures, designed with alternate donor and acceptor groups arranged in a radially D-A-D structure. These emitters are characterized by a notably short delayed lifespan (~100 ns) because of the formation of delocalized excited state induced by the linear D-A-D structure and strong SOC by distinct excited state character of $S_1$ and $T_1$, which promote $T_1$-to-$S_1$ spin-flip process. Both emitters have been utilized to fabricate efficient OLEDs, achieving an EQE of 13.0% for green emission and 9.1% for sky-blue emission. Particularly, the devices demonstrate exceptionally low efficiency roll-off, a result of the rapid $T_1$-to-$S_1$ flip process that suppresses triplet exciton annihilation. The EQE roll-offs from the maximum to 1000, 5000, and 10,000 cd/m$^2$ are correspondingly 3.8%, 21%, and 33% for the green OLED, and 13%, 35%, and 46% for the sky-blue OLED. These observations confirm the effectiveness of our molecular design strategy in enhancing the spin-flip process and improving the roll-off performance of OLEDs, showcasing the potential of these materials for high-performance display and lighting applications.

## Declaration of competing interest

The authors declare that they have no known competing financial interests or personal relationships that could have appeared to influence the work reported in this paper.

## CRediT authorship contribution statement

**Zhaoyue Lü:** Writing – original draft, Supervision, Investigation, Data curation, Conceptualization. **Tiantian Chai:** Writing – original draft, Data curation. **Yichao Jin:** Writing – original draft, Data curation. **Xiao Wang:** Data curation. **Ye Zou:** Writing – review & editing, Conceptualization. **Lijiang Zhang:** Data curation. **Jiankang Feng:** Data curation. **Mengtong Zhang:** Data curation. **Shuo Wang:** Data curation. **Chichong Lu:** Writing – original draft, Investigation, Conceptualization. **Guofan Jin:** Writing – review & editing, Writing – original draft, Supervision, Investigation, Conceptualization.

## Acknowledgment

This work was financially supported by the National Natural Science Foundation of China (Nos. T2441002 and 22175186).

## Supplementary materials

Supplementary material associated with this article can be found, in the online version, at doi:10.1016/j.cclet.2025.110817.

## References

[1] Y. Lee, H. Cho, H. Yoon, et al., Adv. Mater. Technol. 8 (2023) 2201067.
[2] G. Hong, X. Gan, C. Leonhardt, et al., Adv. Mater. 33 (2021) 2005630.
[3] C.M. Kang, H. Lee, J. Inf. Disp. 23 (2022) 19–32.
[4] W.J. Joo, J. Kyoung, M. Esfandyarpour, et al., Science 370 (2020) 459–463.
[5] Y. Lee, J.W. Chung, G.H. Lee, et al., Sci. Adv. 7 (2021) eabg9180.
[6] H. Chae, Y. Park, Y. Jo, et al., Adv. Mater. Interfaces 10 (2023) 2202443.
[7] X. Hu, Y. Qin, Z. Li, et al., Chin. Chem. Lett. 33 (2022) 4645–4648.
[8] X.C. Fan, K. Wang, Y.Z. Shi, et al., SmartMat 4 (2023) e1122.
[9] S. Hirata, Y. Sakai, K. Masui, et al., Nat. Mater. 14 (2015) 330–336.
[10] Y. Mei, D. Liu, J. Li, H. Li, W. Wei, J. Mater. Chem. C 9 (2021) 5885–5892.
[11] H. Uoyama, K. Goushi, K. Shizu, H. Nomura, C. Adachi, Nature 492 (2012) 234–238.
[12] Y. Im, M. Kim, Y.J. Cho, et al., Chem. Mater. 29 (2017) 1946–1963.
[13] F. Fang, L. Zhu, M. Li, et al., Adv. Sci. 8 (2021) 2102970.
[14] Y. Mei, D. Liu, J. Li, J. Wang, J. Mater. Chem. C 10 (2022) 16524–16535.
[15] X. Dong, S. Shen, Y. Qin, et al., Chin. Chem. Lett. 34 (2023) 108311.
[16] J. Liu, Z. Feng, C. Peng, et al., Chin. Chem. Lett. 34 (2023) 107634.
[17] L. Yan, N. Su, Y. Yang, et al., SmartMat 5 (2024) e1272.
[18] M. Mamada, H. Katagiri, C.Y. Chan, et al., Adv. Funct. Mater. 32 (2022) 2204352.
[19] J. Kim, C.W. Joo, S.J. Woo, et al., J. Mater. Chem. C 10 (2022) 7304–7310.
[20] D. Zhang, M. Cai, Y. Zhang, D. Zhang, L. Duan, Mater. Horiz. 3 (2016) 145–151.
[21] H. Noda, H. Nakanotani, C. Adachi, Sci. Adv. 4 (2018) eaao6910.
[22] C.Y. Chan, M. Tanaka, H. Nakanotani, C. Adachi, Nat. Commun. 9 (2018) 5036.
[23] S. Zou, F. Xie, M. Xie, et al., Adv. Sci. 7 (2020) 1902508.
[24] F.M. Xie, Z.D. An, M. Xie, et al., J. Mater. Chem. C 8 (2020) 5769–5776.
[25] C. Chan, M. Tanaka, Y. Lee, et al., Nat. Photonics 15 (2021) 203–207.
[26] C. Murawski, K. Leo, M.C. Gather, Adv. Mater. 25 (2013) 6801–6827.
[27] M. Hasan, A. Shukla, V. Ahmad, et al., Adv. Funct. Mater. 30 (2020) 2000580.
[28] B. Zee, Y. Li, G.J.A.H. Wetzelaer, P.W.M. Blom, Adv. Opt. Mater. 9 (2021) 2100249.
[29] Y. Liu, C. Li, Z. Ren, S. Yan, M.R. Bryce, Nat. Rev. Mater. 3 (2018) 18020.
[30] T. Hosokai, H. Matsuzaki, H. Nakanotani, et al., Sci. Adv. 3 (2017) e1603282.
[31] X. Dai, L. Liu, Z. Ji, Q. Meng, Y. Zou, Chin. Chem. Lett. 34 (2023) 107239.
[32] Y. Zou, Q. Meng, H. Mao, D. Zhu, Org. Electron. 41 (2017) 307–314.
[33] J. Chen, Y. Xiao, K. Wang, et al., Angew. Chem. Int. Ed. 60 (2021) 2478–2484.
[34] W. Li, M. Li, W. Li, et al., ACS Appl. Mater. Interfaces 13 (2021) 5302–5311.
[35] L. Gan, Z. Xu, Z. Wang, et al., Adv. Funct. Mater. 29 (2019) 1808088.
[36] M.J. Frisch, G.W. Trucks, H.B. Schlegel, et al., Gaussian 16 Revision A.03, Gaussian Inc., Wallingford, CT, 2016.
[37] R.L. Martin, J. Chem. Phys. 118 (2003) 4775–4777.
[38] Y. Liu, P. Ganesan, M. Chen, et al., Chem. Eng. J. 499 (2024) 156529.
[39] J.U. Kim, I.S. Park, C.Y. Chan, et al., Nat. Commun. 11 (2020) 1765.